www.czasopisma.pan.pl PAN POLSKA AKADEMIA NAUK www.journals.pan.pl

Arch. Metall. Mater. **66** (2021), 1, 187-195

DOI: 10.24425/amm.2021.134775

E. HAJIBABA GOZARGANJI[1], A. FARNIA[1*], M. EBRAHIMNIA[1]

EFFECT OF SHIELDING GAS COMPOSITION ON GEOMETRY AND AUSTENITE FORMATION IN LOW POWER PULSED Nd:YAG LASER WELDED 2205 DUPLEX STAINLESS STEEL

This paper presents an investigation into effect of nitrogen content of shielding gas mixture on weld geometry, microstructure and hardness of pulsed laser welded 2205 duplex stainless steel. Full penetration autogenous welding was performed on 2 mm thick plates using a low power pulsed Nd: YAG laser. light and scanning electron microscopy were used to study the resulting microstructures. It is observed that 2 mm full penetrated joint decreases to 1.8 mm by dominating nitrogen in argon-nitrogen mixture. Different morphologies of austenite phase as well as an increase of 8% of its content can be observed in pure nitrogen shielded welds. Average weld grain size in sample which is welded in nitrogen atmosphere stands at approximately 41 μm which is smaller than that of argon atmosphere which is about 51 μm. Micro-hardness test reveals that hardness values increase from 280 HV in base metal to 307 HV in weld center line and the shielding gas mixture does not significantly influence the weld hardness.

Keywords: low power pulsed Nd:YAG laser welding, duplex stainless steel, shielding gas, nitrogen, austenite formation

1. Introduction

Duplex stainless steels have been extensively used in different industries recently due to their good strength and corrosion resistance. These excellent properties are attributed to simultaneous presence of ferrite and austenite, and also minimum amount of secondary phases in their microstructures [1]. In these alloys ferrite offers stress corrosion cracking (SCC) resistance, while austenite provides ductility and general corrosion resistance [2]. Among these stainless steels, grade 2205 has vast applications in different industries such as petrochemical, marine, and nuclear industries. An important issue that should be considered in duplex alloys is ferrite/austenite ratio which should be near to 1:1 value. This ratio is generally achievable in wrought duplex stainless steels by adding proper alloying elements or selecting appropriate post weld heat treatment [3,4]. 2205 alloy as a typical duplex stainless steel, thoroughly solidify into ferrite, and then during cooling to room temperature, ferrite transforms partially into austenite through a solid-state transformation. In other words, the higher the cooling rate, the fewer austenite is formed due to lack of time for diffusion [1,5].

However, welding due to its high cooling rates, has a negative impact on dual phase balance and results in an unbalanced fusion zone which comprise a sizeable amount of ferrite [1,5-7]. This effect could be even worse in high energy beam processes such as electron beam welding (EBW) or laser beam welding (LBW) due to their lower heat input and consequent higher cooling rates [1]. Saravanan et al. [8] studied the effect of laser welding heat input on macro- and microstructure of a duplex stainless steel. They exhibited the amount of ferrite phase increases by increasing heat input values. Verma and Taiwade in a review paper [9] showed that many scientists have investigated the effect of heat input on duplex stainless steel microstructure and mechanical properties in various welding processes. Nevertheless, LBW process due to its great advantages is appealing for researchers to be investigated further on different types of alloys. In fact, thanks to high power density of this process, less distorted narrow and deep penetrated joints can be achievable, so sheets can be welded with a single pass without beveling and/or using filler metals although bevel preparation must be substantially precise. This could lead to a good productivity [2]. In comparison with continuous laser welding pulsed laser welding offers a couple of advantages such as significant lower heat input and lower HAZ width and lower residual stresses [10]. As during pulsed operation of Nd:YAG laser, energy is delivered through intermittent pulses which can be controlled for duty cycle (on-off time), frequency and pulsed energy.

[1] DEPARTMENT OF MATERIALS ENGINEERING, SCIENCE AND RESEARCH BRANCH, ISLAMIC AZAD UNIVERSITY, TEHRAN, IRAN

* corresponding author: a.farnia@srbiau.ac.ir

Ferrite to austenite ratio is the most important issue which should be taken into consideration, in welding of duplex stainless steel. To prevent excessive decrease of austenite content in weld metal, different studies have been conducted. For instance, one of the basic ways to improve austenite content in weld metal is using filler metals instead of autogenous welding [11]. Adding metal powders such as nickel during autogenous welding is reported as another applicable way to boost austenite content in weld zone of power beam welded samples [12,13]. Post weld heat treating (PWHT) was also reported to be a useful method to enhance α/γ ratio in autogenous pulsed laser welding of super duplex stainless steel due to secondary austenite formation during PWHT [14]. In addition to these methods, there are some researches who investigate effects of nitrogen shielding gas not only on austenite formation of weld metal but also on weld geometry in continuous laser welding processes [15]. Verbai et al. [16] revealed that addition of nitrogen to the shielding gas mixture could prevent nitrogen loss in weld metal. They showed that nitrogen level plays a significant role in amount of austenite formation. Weld metal through shielding gas was also reported as another feasible method to raise austenite percentage in weld metal [17,18].

Although there are many worthy studies on effect of laser parameters on weld geometry as well as optimizing the laser welding parameters [19,20], there are few investigations regarding effects of shielding gas composition on pulsed laser welding of duplex stainless steel joints. Therefore current study is organized to investigate effects of nitrogen content of argon-nitrogen mixture as shielding gas on macrostructure, microstructutre and micro-hardness of an autogenously pulsed Nd:YAG laser welded 2205 duplex stainless steel joint. In this way, the effect of nitrogen content on weld geometry, weld metal grain size, HAZ formation, austenite content and its different probable morphologies are fully discussed.

2. Materials and method

Duplex stainless steel (2205) with the chemical composition which is obtained by an Oxford optical emission spectroscopy (OES)-model Foundary Master UV and shown in Table 1 was used for this research.

TABLE 1

Chemical composition of 2205 duplex stainless steel (wt%)

%Fe	%C	%Mn	%P	%S	%Si	%Cr	%Ni	%Mo	%Cu
Base	0.014	1.48	0.016	0.009	0.40	22.25	5.30	3.07	0.24

100 mm×65 mm×2 mm plates are used for butt weld joints. To achieve a smooth surface with high precision, all edges that are subjected to laser welding are cut out by wire cut process. In order to remove the thin oxide layer which is formed during wire cut process, immediately prior to welding all edges are sandpapered with fine sand papers and then are cleaned by acetone. Laser equipment that was used for this study is a IQL-10 pulsed Nd:YAG laser with 150 mm and 1.5 mm focal distance and focal spot, respectively. It can produce pulses with the duration of 0.5 to 20 ms, and with the frequency of 1 to 200 Hz. Maximum laser average power is 500 W. All welding experiments are performed in a flat position. In order to fix samples tightly to each other a fixture is used. All joints are welded autogenously, and fully penetrating joints are achieved by a single pass welding whose parameters are listed in table 2.

TABLE 2

Laser parameters for achieving full weld penetration

Average Power (W)	Frequency (Hz)	Pulse Duration (ms)	Welding Speed (mm/s)	Overlapping Factor	Peak Power (KW)	Pulse Energy (J)
225	7	18	1.9	82	1.78	32.14

Overlapping factor and Peak power are calculated based on Equation. 1 and Equation 2, respectively [21].

$$O_f = \left(1 - \frac{\frac{v}{f}}{D + vW}\right) \times 100 \tag{1}$$

$$P_p = \frac{P_{ave}}{fW} \tag{2}$$

Where O_f is overlapping factor, v is travel speed, f is frequency, W is pulse duration, D is laser spot size, P_{ave} is average power and P_p is peak power which is considered 1.5 mm which is obtained from the used laser parameters shown in table 2.

In order to shield weld metal and heated surface during welding, different argon-nitrogen shielding gas compositions as shown in table 3 are used through a coaxial nozzle with a flow rate of 20 L/min.

TABLE 3

Shielding gas composition and flow rate

Sample No.	Shielding gas	Flow Rate
1	100% Argon	20 L/Min
2	75% Nitrogen+25%Argon	20 L/Min
3	100%Nitrogen	20 L/Min

In order to microstructural studies, samples preparation was performed utilizing sandpaper grounding up to 2000-grit sandpaper followed by polishing with 0.5 microns diameter Al_2O_3 particle suspension solution. Etching solutions for macro and micro evaluation are super kalling and KOH electrolyte respectively. Weldments were then investigated in terms of macro and microstructures by light and EDS-equipped field emission scanning electron microscopes. Each weld line was randomly cross-sectioned from three different locations. The cross sections were observed microscopically to examine the possibility of presence of any cracks and pores. Austenite content in weld

zone, and average weld grain size are calculated by utilizing Microstructural Image processing (MIP) software, respectively. Two samples which are welded in pure argon and pure nitrogen were subjected to micro-hardness test. The micro-hardness test was carried out using a Shobsary- model N5 micro-hardness Tester apparatus. The load of 300 gr-N was applied for 15 seconds on the weldment region as well as the base metal.

3. Results and discussion

3.1. Macrostructure

Effect of nitrogen content of shielding gas on welds cross section are shown in Fig. 1(a), (b) and (c). As it is shown, the shielding gas composition directly affects weld profile. As it can be seen obviously from the picture, considering the scale bar, the weld root width is measured nearly 200 microns above the lowest point of the weld zone. It is observed that in constant laser welding parameters, when nitrogen concentration increased in shielding gas mixture, width of weld beads increases from 1.57 mm in pure argon shielding gas (Fig. 1(a)) to 1.71 mm in pure nitrogen atmosphere (Fig. 1(c)) while weld root width show a decline from 0.71 mm in pure argon atmosphere to 0.46 mm in pure nitrogen shielding gas. Bauer et al. [15] revealed that the shielding gas mixture significantly affects joint geometry. They, as well, showed using Argon as shielding gas increases the weld root width in compare with that when Nitrogen gas is used. This is in good agreement with the findings of this study. In addition, weld surface in pure argon shielding is slightly concave while other samples show rather convex surfaces.

Fig. 2 demonstrates the weld various dimensional changes trends as nitrogen content of the shielding gas increases. One may see that the weld face width as well as its depth increases as nitrogen content of shielding gas increases. Reversely, the root width of the weld decreases by increasing the Nitrogen content of shielding gas.

Furthermore, rising nitrogen content in gas mixture does not increase the probability of porosity formation and all welds were sound and free of porosity based on cross-sectional observations, as was explained earlier.

On the other hand, increasing nitrogen content in shielding gas mixture, leads to an important phenomenon which is a reduction in welds' depth of penetration. In fact, by dominating

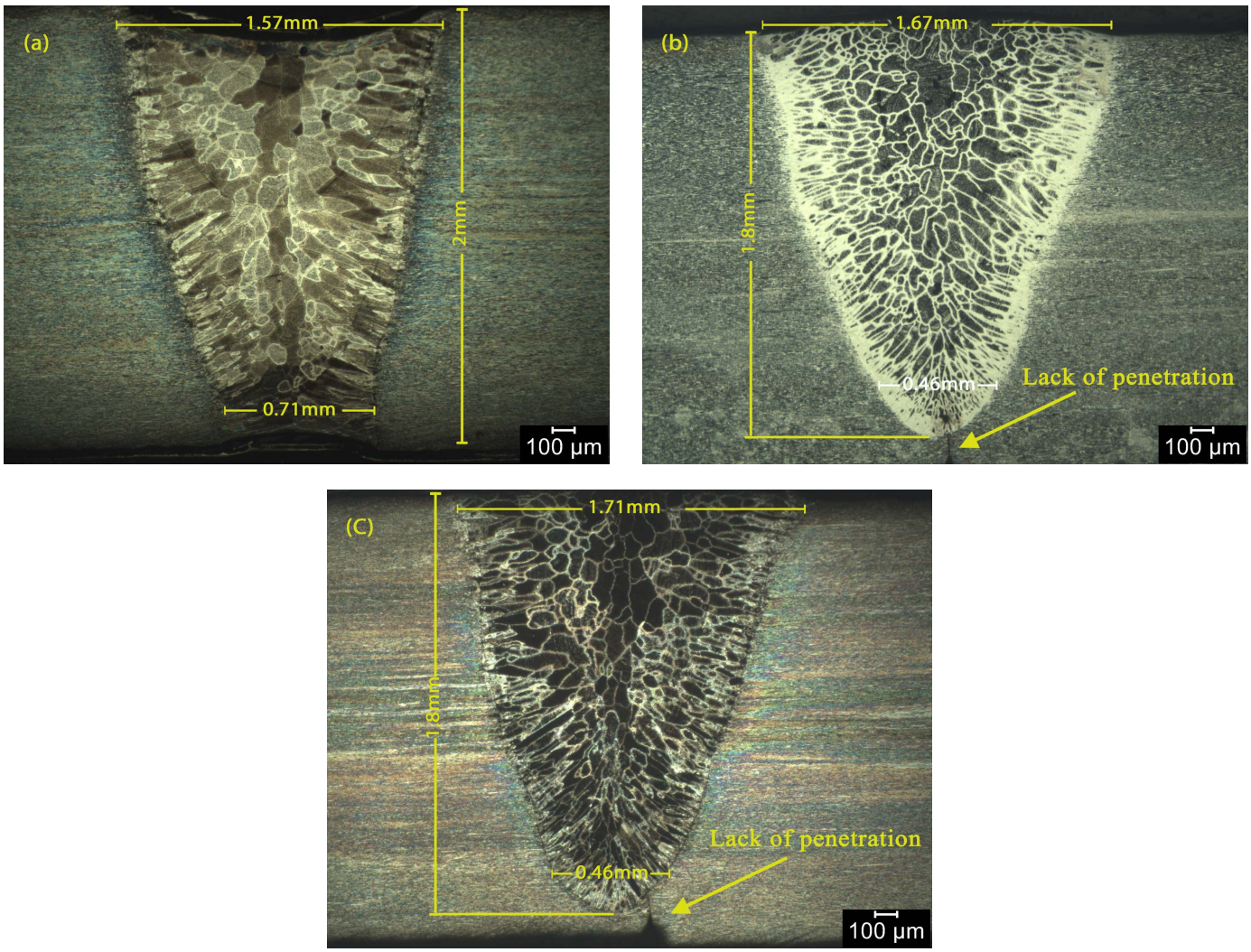

Fig. 1. Weld macrographs, (a) 100% Argon shielded sample, (b) 75% N_2+25% Argon shielded sample, (c) 100% Nitrogen shielded sample

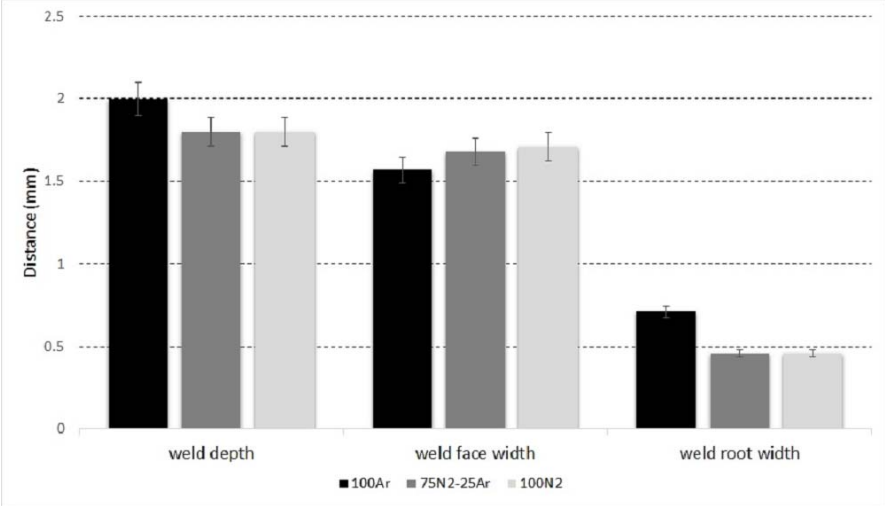

Fig. 2. Changes in weld sizes with changing the shielding gas composition

nitrogen concentration in argon-nitrogen mixture, depth of penetration which is 2 mm in argon shielding atmosphere declines to 1.8 mm in nitrogen shielding atmosphere.

During laser welding there are two kinds of atmosphere between laser nozzle and base metal. One is related to metallic evaporation from keyhole formation in base metal that contribute to metal plume, and the other one is the so-called gas plasma atmosphere which is formed by ionization of shielding gas [22]. Due to this fact, shielding gas could play an important role in the intensity of incident laser beam. Intensity of the incident laser beam is calculated by the following equation [23]:

$$I(h) = I_0(1 - R)e^{-\alpha h} \tag{3}$$

Where $I(h)$ is the intensity of laser when it approaches base metal surface, I_0 is primary laser intensity, R is laser beam reflection coefficient, α is the inverse Bremsstrahlung absorption coefficient, and h is the height of laser beam and plasma fusion zone. According to this equation, ionization potential of shielding gas can directly affect the intensity of laser beam. In other words, gas lower ionization potential results in easier dissociation of its atoms and facilitate formation of gas plasma which flows up to the laser beam and in interaction with laser beam reduces its intensity [22,23]. Argon ionization potential energy is lower than that of nitrogen [24]. According to above mentioned facts when nitrogen percentage increases and becomes the dominant element in argon-nitrogen mixture, mean ionization potential for gas mixture decreases so laser intensity declines and this results in a reduction of weld depth. Rul Lai et al. [17] concluded that nitrogen has no effect on depth of penetration in continuous laser welding. This contrast can be attributed to the differences between natures of pulsed and continuous lasers. In fact, in pulsed lasers the heat source is on only for a short limited time which results in a reduction in effective power density as well as interaction time [21]. Due to this fact, role of gas plasma in reducing laser beam intensity becomes bolder which results in less penetrated weld joints. However, sample that welded in pure argon shielding gas experienced full penetration weld.

3.2. Microstructure

Base metal microstructure is shown in Fig. 3. Due to special thermomechanical process used to produce such materials the resulted microstructure consists of approximately equal amount of ferrite and austenite. It can be seen from the Fig. 3 that austenite phase distributes evenly through ferrite matrix in a pan-cake form and has distinct grain boundaries with the matrix.

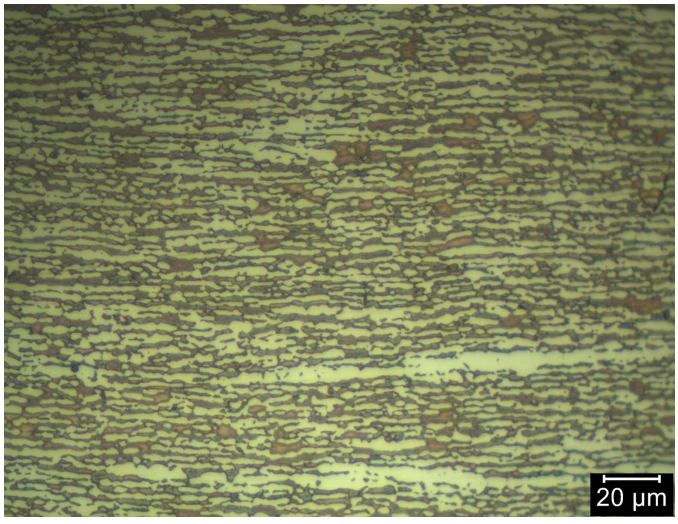

Fig. 3. Microstructure of 2205 duplex stainless steel (pan-cake form microstructure of ferrite and austenite)

Weldments microstructure is shown in Fig. 4. As this picture demonstrates, because of the complicated thermal cycles that base metal experienced during welding, its unique microstructure is being thoroughly destroyed, and wrought fine grain microstructure in base metal converts to a solidified microstructure with coarser grains that comprise of columnar and equiaxed grains.

Duplex stainless steels solidify into primary δ ferrite, then during cooling to room temperature and through a solid-state

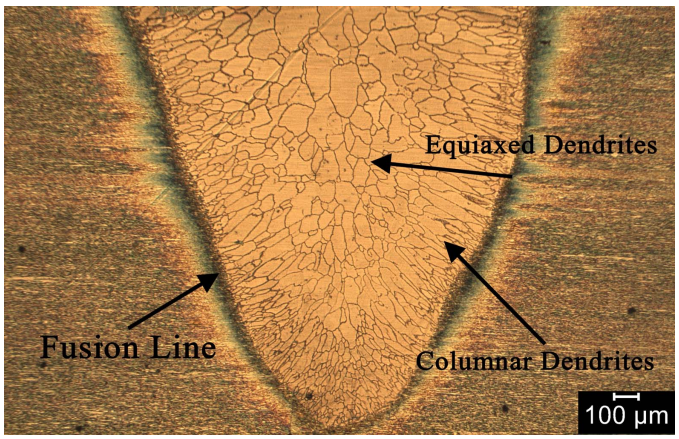

Fig. 4. Weldment microstructure

transformation ferrite transform partially to austenite [13,25]. This transformation occurs in three different morphologies, first as grain boundary austenite, second as Widmanstätten austenite, and finally as intragranular austenite whose driving forces increase from the first two kinds of austenite to the third one [17]. Different morphologies of austenite are mostly due to the change in the cooling rate, which changes the mechanism of nucleation and growth of austenite during the phase transformation. Austenite nucleates preferentially on the prior ferrite grain boundaries. During slow cooling rate, an equiaxed grain morphology is formed. Widmanstätten morphology of austenite is obtained by high cooling rates. The latter microstructure mostly consists of allotriomorphic and elongated intragranular austenite. The allotriomorphic austenite is obtained at an early stage of transformation (i.e., at lower undercooling), while the intragranular austenite is transformed at a comparatively higher undercooling (i.e., in the lower temperature regime) [26].

Figure 5(a) and (b) show these types of austenite morphologies in the weld zone of the sample welded in pure nitrogen shielding atmosphere. Widmanstätten and especially intragranular austenite are less likely to form in pure argon atmosphere and the grain boundary austenite is the dominant austenite morphology in the weld metal of 100%Ar shielded weld sample (Fig. 5 (c)).

Due to higher cooling rates in welding, there is not enough time for formation of austenite so the amount of austenite falls sharply in weld zone and α/γ ratio increases.

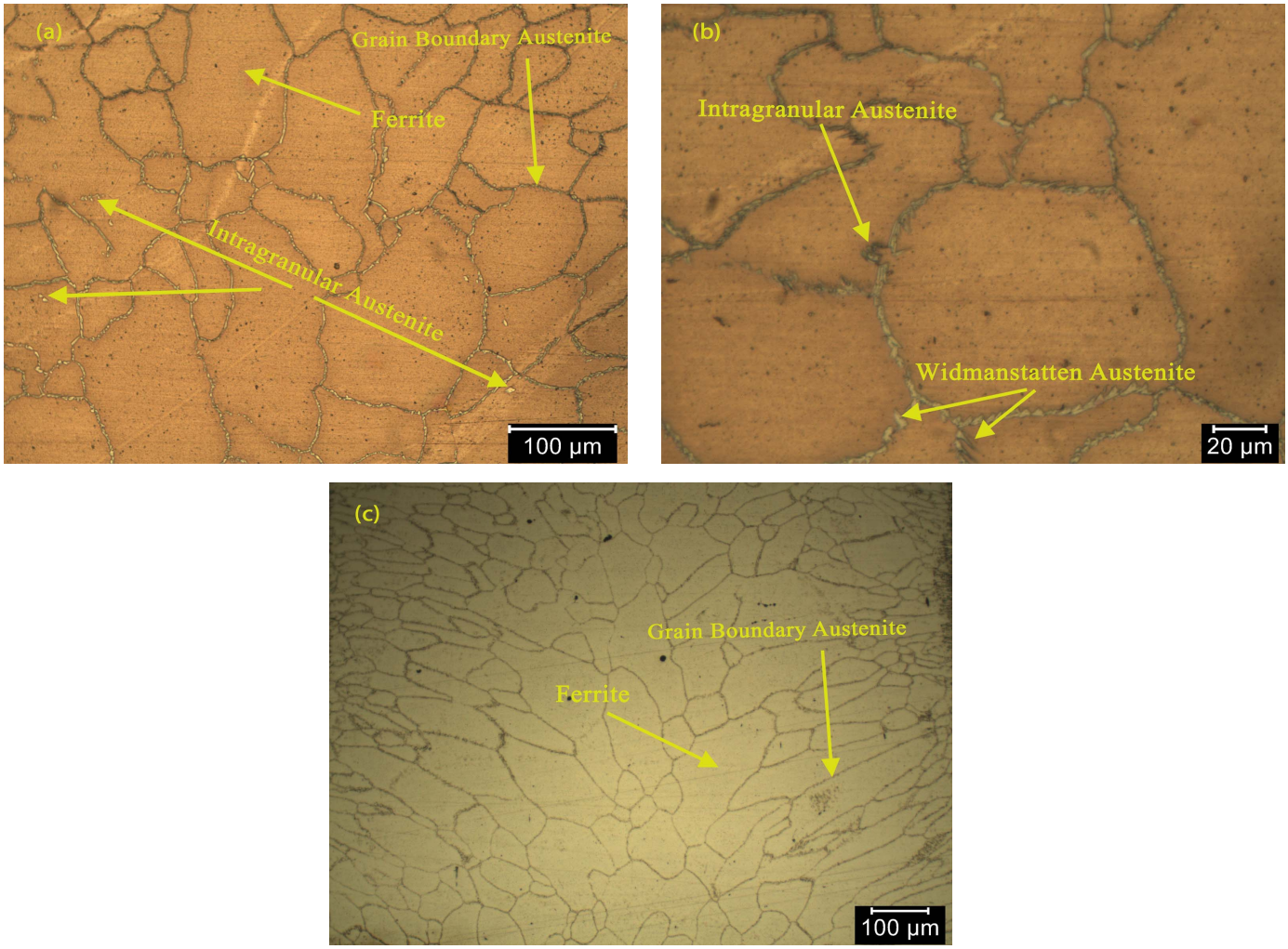

Fig. 5. Weld microstructure in different shielding gas compositions; (a) intragarnular and grain boundary Austenite in 100% Nitrogen shielded sample, (b) Widmanstätten Austenite in 100% Nitrogen shielded sample, (c) grain boundary Austenite in 100% Argon shielded sample

Obtained results by image analyzer software revealed that austenite content in the sample which is welded with pure nitrogen as shielding gas, increases by 8% compared to the sample which is welded in pure argon atmosphere. These results show that replacing argon with nitrogen as shielding gas cause an important phenomenon in weld microstructures. Since nitrogen known as austenite promoter, absorption of nitrogen in weld pool could contribute to more austenite formation in weld zone [14,15]. Absorbed nitrogen shifts the austenite solvus line to higher temperatures [11]. On the other hand, by increasing nitrogen content austenite tends to nucleate intragranularly at higher temperatures. Because the nitrogen atoms diffuse more rapidly and the moving distance of nitrogen atoms under the ferrite solvus temperature becomes shorter [9].

One can see from Fig. 6(a) that the austenite phase forms in grain boundary morphology in 100%Ar shielded weld metal while other forms of austenite like as finger-like intraganular austenite are more likely to form when pure nitrogen used as shielding gas, as can be seen in Fig. 6(b). The distinct intragranular austenite phase could be created through heterogeneous nucleation. They could be the nucleated plates extended on the grain boundaries which are not observable in the cross section of the plane. Though, the formation mechanism, from the films of allotriomorphic nature, for the morphologies of the finger-like austenite is still debatable [26].

Moreover, comparing samples' micrographs shows that the sample which is welded with pure nitrogen shielding gas benefits from smaller ferrite grain size compared to the one welded with pure Argon. Grain size measurements obtained by image analyzer software reveal that average ferrite grain size in weld metal of 100%N_2 shielded weld sample is approximately 29 μm while this value 100%Ar shielded weld sample is about 40 μm. The histograms of grain size distribution are presented in Fig. 7(a) and (b) for N_2 shielded and Ar shielded weld samples, respectively. This decline in average ferrite grain size in 100%N_2 shielded weld sample, as it can be found from Fig. 1 as well, can be attributed to the fact that when welding was performed in presence of nitrogen instead of argon, austenite tends to nucleate intragranularly at high temperatures which restricts ferrite grain growth [9]. By reducing ferrite grain size, length of grain boundaries increases simultaneously which means that main areas for austenite nucleation increase that lead to higher austenite amount in 100%N_2 shielded weld sample.

Furthermore, microstructure survey showed that intermetallic phases such as sigma and chi, carbides or nitrides were not formed during and after welding in both argon and nitrogen protected samples. This can be due to high cooling rates of pulsed laser welding [2].

As mentioned previously, due to high intensity and low heat input of laser beam, generally laser beam welding lead to a narrow heat affected zone. In pulsed laser welding HAZ becomes even narrower due to nature of pulses. Fig. 8 (a) and (b) shows fusion lines of 100%Ar and 100%N_2 shielded weld samples, respectively. As it can be seen, the microstructure of base metal is remained unchanged up to the fusion line and fusion lines are very narrow in both samples. Based on these observations, one may conclude that there is not any distinguishable

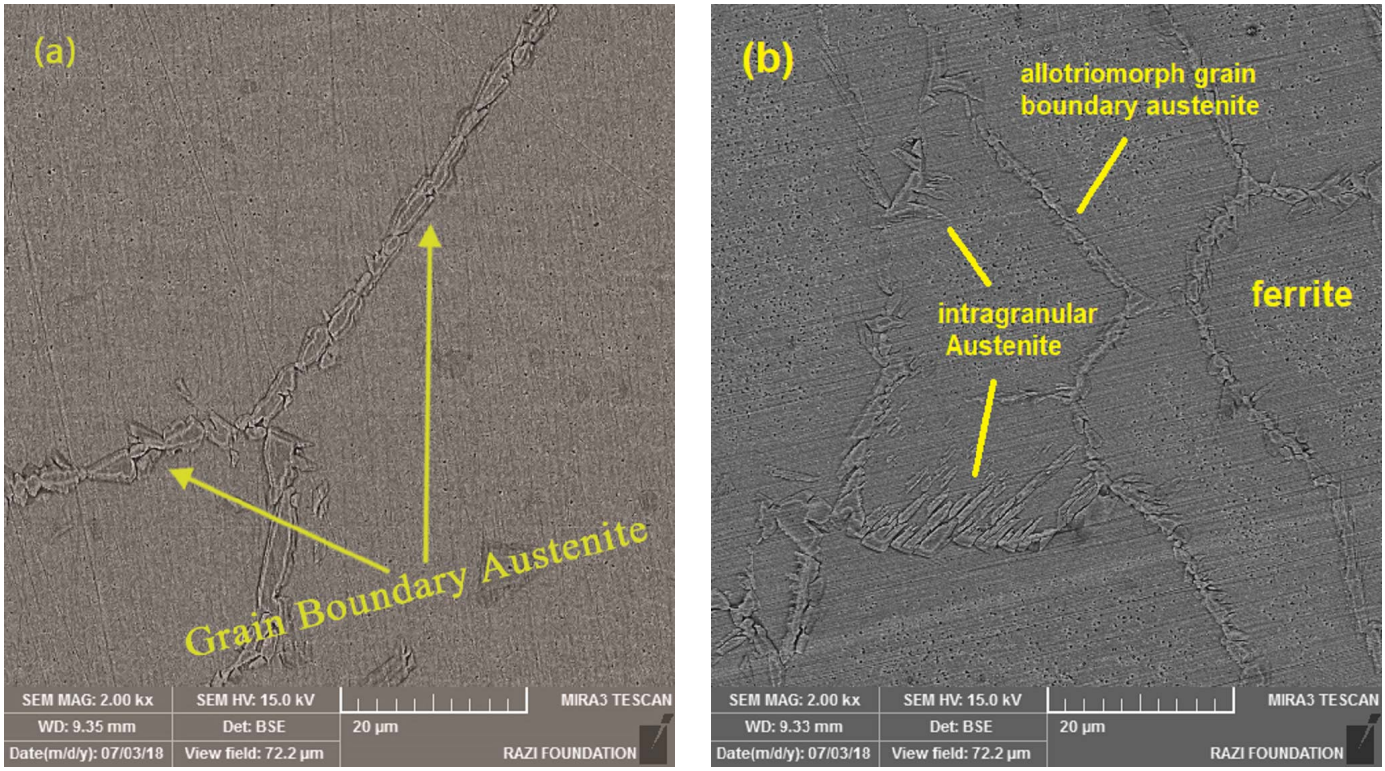

Fig. 6. FESEM Pictures of the austenite morphology in different shielding gas compositions; (a) grain boundary Austenite in 100% Argon shielded sample; (b) intragranular Austenite formation in 100% Nitrogen shielded sample

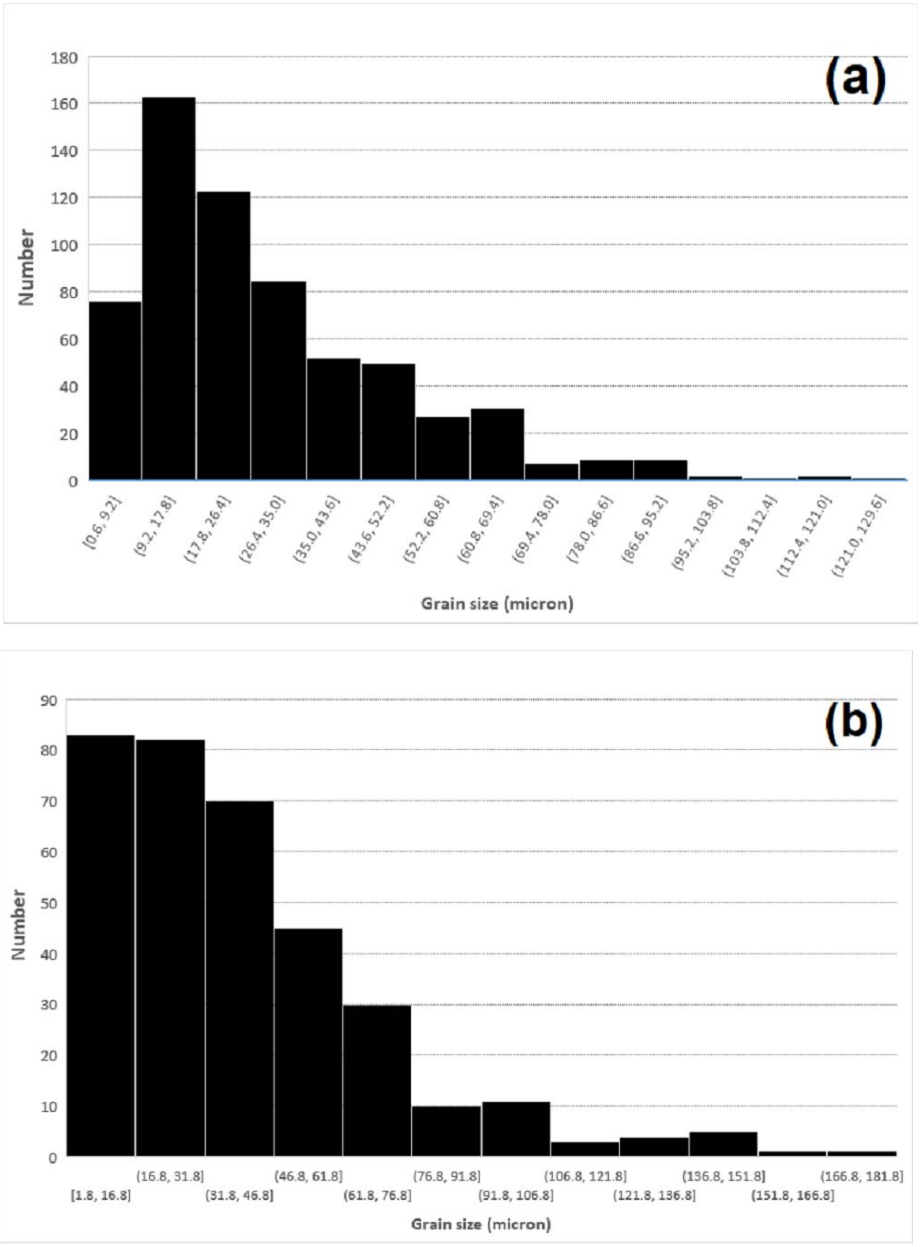

Fig. 7. Histograms of grain size distribution for, (a) 100% Nitrogen shielded sample, (b) 100% Argon shielded sample

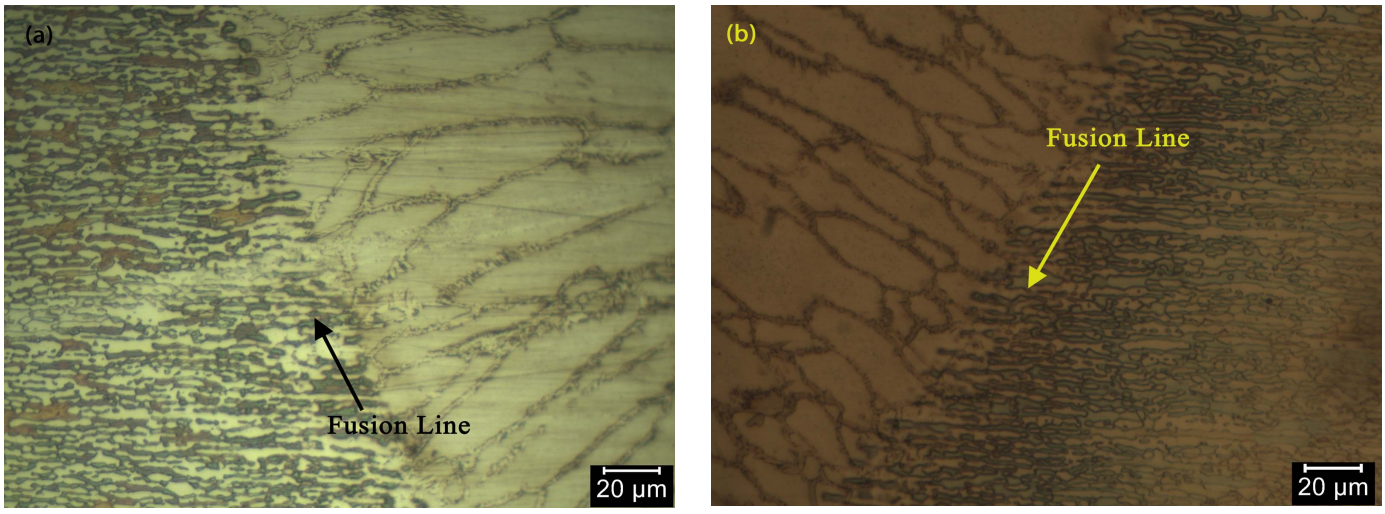

Fig. 8. Micrographs of fusion line in, (a) 100% Argon shielded sample, (b) 100% Nitrogen shielded sample

region between base metal and fusion line in both samples. In others words, fusion line immediately connects to base metal without any noticeable grain growth which is the characteristic of heat affected zone. This is due to high cooling rate nature of pulsed laser welding which does not allow grains to stay at temperatures higher than ferrite solvus temperature for a long time, which results in especially fine grain microstructure in fusion line. Also it may be concluded that shielding gas composition has no effect on HAZ breadth and microstructure in this set of experiments.

Hardness measurements:

Micro-hardness results showed an increase in hardness values from base metal to center of weld metal in both samples, as shown in Fig. 9.

As it was mentioned previously, weld microstructure is solidified type which is totally different from base metal. Due to high cooling rate of pulsed laser welding, there is not enough time for austenite to nucleate from ferrite grain boundaries and this cause an unbalanced α/γ ratio with high amount of ferrite which results in a weld with higher hardness values in comparison with base metal [1,15]. In addition to this, hardness values in samples that were welded in pure argon and nitrogen do not show great differences with each other. In fact, as it was noticed before, weldment that is welded in pure nitrogen atmosphere benefits from higher austenite content which should result in relatively lower values of hardness compared to weldments in argon atmosphere. However, lower average grain size can somewhat compensate for the decline in hardness values in 100%N_2 shielded weld sample.

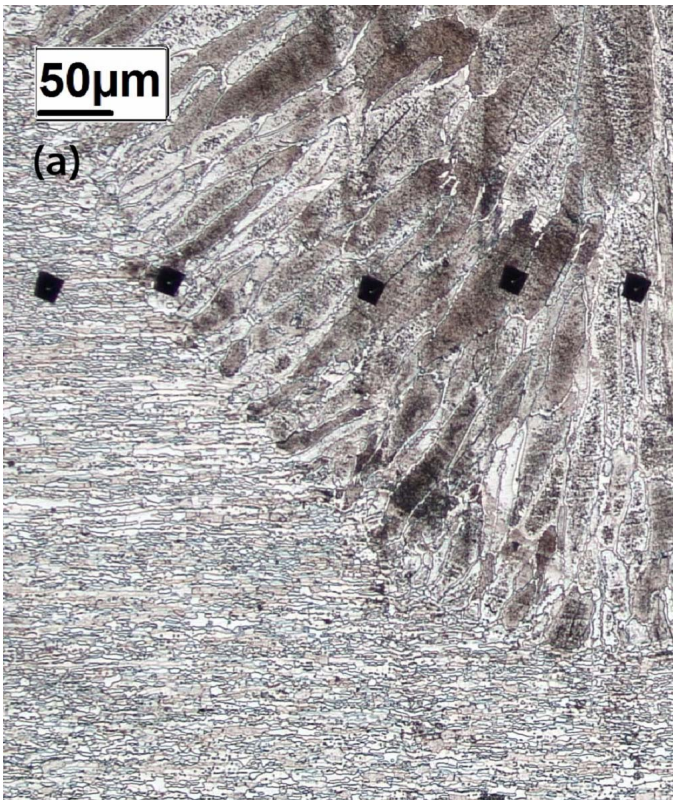

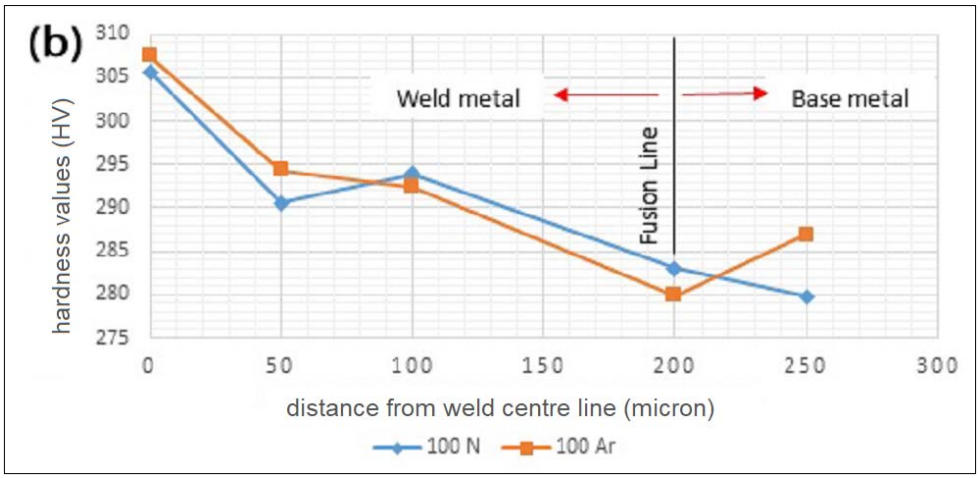

Fig. 9. Micro-hardness results, (a) Areas of tests, (b) Micro-hardness profile

4. Conclusions

Adding nitrogen to weld metal is quite feasible in pulsed laser welding of duplex stainless steels. Although absorbed nitrogen in weld metal was not too much, it played a crucial role in weldment in terms of both micro and macro structures. Nitrogen, due to its lower ionization potential, reduces laser beam intensity that results in beam's lower penetration. Absorbed nitrogen in weld metal not only increases austenite content of weld metal but it also promotes formation of other austenite morphologies such as Widmanstätten and intragranular austenite in comparison with grain boundary morphology austenite which is formed in pure argon shielded weld metal microstructure. Welding in nitrogen atmosphere results in a finer grain weld metal compared to argon protected weld. Heat affected zone can be negligible in both 100%Ar and100%N_2 shielded weld samples. Micro-hardness test reveals that hardness values increase from 280 HV in base metal to 307 HV in weld center line. There are no significant differences in micro-hardness values of samples which are welded in pure argon and pure nitrogen atmosphere.

REFERENCES

[1] G.S. Crespo, J.L. Padilha, C.R. Sokei, R.C. Tokimatsu, J. Gallego, V.A. Ventrella, Mater. Sci. Forum. **869**, 458-463 (2016).

[2] M. Bolut, C.Y. Kong, J. Blackburn, K.A. Cashell, P.R. Hobson, Phys. Procedia. **83**, 417-425 (2016).

[3] R. Soltysiak, T. Gietka, A. Soltysiak, Adv. Mech. Eng. **10** (1), 1-12 (2018).

[4] K. Yurtisik, S. Tirkes, I. Dykhno, C. Hakan Gur, R. Gurbuz, Soldag. insp. **18** (3), 207-216 (2013).

[5] F. Mirakhorli, F. Malek, M.J. Torkamany, J. of Materi. Eng. and Perform. **21**, 2173-2176 (2012).

[6] G. Sivakumar, S. Saravanan, K. Raghukandan, Optik **131**, 1-10 (2017).

[7] Y. Yang, B. Yan, J. Li, J. Wang, Corros. Sci. **53**, 3756-3763 (2011).

[8] S. Saravanan, N. Sivagurumanikandan, K. Raghukandan, Optik. **185**, 447-455 (2019).

[9] J. Verma, R. V. Taiwade, J. Manuf. Process. **25**, 134-152 (2017).

[10] Q. Sun, H. S. Di, J.C. Li, X.N. Wang, Mater. Des. **105**, 201-211 (2016).

[11] J.C. Lippold, D.J. Kotecki, Welding Metallurgy and Weldability of Stainless Steels, wiley publications, (2005).

[12] H.C. Wu, L.W. Tsay, C. Chen, ISIJ. INT. **44** (10), 1720-1726 (2004).

[13] V. Muthupandi, P. Bala Srinivasan, V. Shankar, S.K. Seshadri, S. Sundaresan, Mater. Lett. **59**(18), 2305-2309 (2005).

[14] S. Saravanan, K. Raghukandan, N. Sivagurumanikandan, J. Manuf. Process. **25**, 284-289 (2017).

[15] B. Bauer, A. Topic, S. Kralj, Z. Kozuh, Mater. Tehnol. **45** (5), 413 (2011).

[16] B. Varbai, T. Pickle, K. Májlinger, intl. J. pressure vessel. Piping. **176**, 103952 (2019).

[17] R. Lai, Y. Cai, Y. Wu, F. Li, X. Hua, J. Mater. Process. Technol. **231**, 397-405 (2016).

[18] M. Keskitalo, K. Mantyjarvi, J. Sundqvist, J. Powell, A.F.H. Kaplan, J. Mater. Process. Technol. **216**, 381-384 (2015).

[19] J. Frostevarg, Opt. Lasers Eng. **101**, 89-98 (2018).

[20] N. Sivagurumanikandan, S. Saravanan, G.Shanthos Kumar, S. Raju, K. Raghukandan, Optik. **157**, 833-840 (2018).

[21] A. Farnia, F. Malek, J. Sabaghzadeh, Opt. Lasers Eng. **51**, 69-76 (2013).

[22] S. Katayama,Y. Kawahito, M. Mizutani, Phy. Procedia **5**, 9-17 (2010).

[23] M. Jokar, F. Malek, M.J. Torkamany, J. Adv. Mater. Processing. **1** (3) 35-42 (2013).

[24] D. Dandas, J.M. Rust, Phys. Rev. A. **71**, 013421(2005).

[25] V. Muthupandi, P. Bala Srinivasan, S. K. Seshadri, S. Sundaresun, Mater. Sci. Eng. A. **358**, 9-16 (2003).

[26] N. Haghdadi, P. Cizek, P.D. Hodgson, V. Tari, G.S. Rohrer, H. Beladi, Acta Mater. **145**, 196-209 (2018).